Article:
Asakura, T., Ogawa, T., Naito, A. et al. (2020) Chain-folded lamellar structure and dynamics of the crystalline fraction of Bombyx mori silk fibroin and of (Ala-Gly-Ser-Gly-Ala-Gly)n model peptides. International Journal of Biological Macromolecules, 164. pp. 3974-3983. ISSN: 0141-8130

https://doi.org/10.1016/j.ijbiomac.2020.08.220

Chain-Folded Lamellar Structure and Dynamics of the Crystalline Fraction of *Bombyx mori* Silk Fibroin and of (Ala-Gly-Ser-Gly-Ala-Gly)$_n$ Model Peptides

Tetsuo Asakura [a]*, Tatsuya Ogawa [a], Akira Naito [a] and Michael P. Williamson [b]

[a] Department of Biotechnology, Tokyo University of Agriculture and Technology, Koganei, Tokyo 184-8588, Japan

[b] Department of Molecular Biology and Biotechnology, University of Sheffield, Firth Court, Western Bank, Sheffield S10 2TN, U.K.

Corresponding author.

E-mail address : asakura@cc.tuat.ac.jp (T. Asakura)

Department of Biotechnology, Tokyo University of Agriculture and Technology,

2-24-16, Nakacho, Koganei, Tokyo 184-8588 JAPAN

Keywords:

Bombyx mori silk fibroin, lamellar structure, ^{13}C CP/MAS NMR, ^{13}C solid-state NMR relaxation time

ABSTRACT

Solid-state NMR is a powerful analytical technique to determine the composite structure of *Bombyx mori* silk fibroin (SF). In our previous paper, we proposed a lamellar structure for Ala-Gly copolypeptides as a model of the crystalline fraction in Silk II. In this paper, the structure and dynamics of the crystalline fraction and of a better mimic of the crystalline fraction, $(Ala\text{-}Gly\text{-}Ser\text{-}Gly\text{-}Ala\text{-}Gly)_n$ (n = 2-5, 8), and ^{13}C selectively labeled [3-^{13}C]Ala-$(AGSGAG)_5$ in Silk II forms, were studied using structural and dynamical analyses of the Ala Cβ peaks in ^{13}C cross polarization/ magic angle spinning NMR and ^{13}C solid-state spin-lattice relaxation time (T_1) measurements, respectively. Like Ala-Gly copolypeptides, these materials have lamellar structures with two kinds of Ala residues in β-sheet, **A** and **B**, plus one distorted β-turn, **t**, formed by repetitive folding using β-turns every eighth amino acid in an antipolar arrangement. However, because of the presence of Ser residues at every sixth residue in $(AGSGAG)_n$, the T_1 values and mobilities of **B** decreased significantly. We conclude that the Ser hydroxyls hydrogen bond to adjacent lamellar layers and fix them together in a similar way to Velcro®.

1. Introduction

The structural analysis of *Bombyx mori* silk fibroin (SF) has received considerable attention because of its supreme physical and medical properties [1-4]. It is remarkable that *B. mori* silkworms can produce such excellent fibers under mild conditions from an aqueous solution at room temperature. By contrast, synthetic materials with comparable elasticity and toughness usually require processing at higher temperatures and/or from less benign non-aqueous solvents [5-9].

The amino acid composition of the heavy chain that comprises most of SF [10-12] is Gly (46 %), Ala (30 %), Ser (12 %), Tyr (5.3 %) and Val (1.8 %). In addition to the fundamental motif $(GA)_m$, the presence of characteristic repeat sequences within the heavy chain was reported by Zhou et al. [13,14]. The primary structure of SF can be approximately divided into four motifs (Figure S1) [14]: a repetitive region containing modules (i), (ii) and (iii), and an amorphous region A (iv) alternate along the chain. Motif (i) consists of a highly repetitive AGSGAG sequence, which constitutes the crystalline regions in SF fibers. The number of occurrences of each $(AGSGAG)_n$ sequence when n = 1-11 and the total numbers of amino acid residues of each $(AGSGAG)_n$ are plotted against n in Figure 1. The total number of AGSGAG sequence repeats is 433 (2,598 amino acid residues). Because the total number of amino acid residues in the heavy chain is 5263, almost half is the AGSGAG sequence. Motif (ii) is less repetitive with mainly hydrophobic residues such as GAGAGY and/or GAGAGVGY which make up the semi-crystalline regions. Motif (iii) is similar to sequence (i) except for the presence of an AAS motif; and motif (iv) makes up the

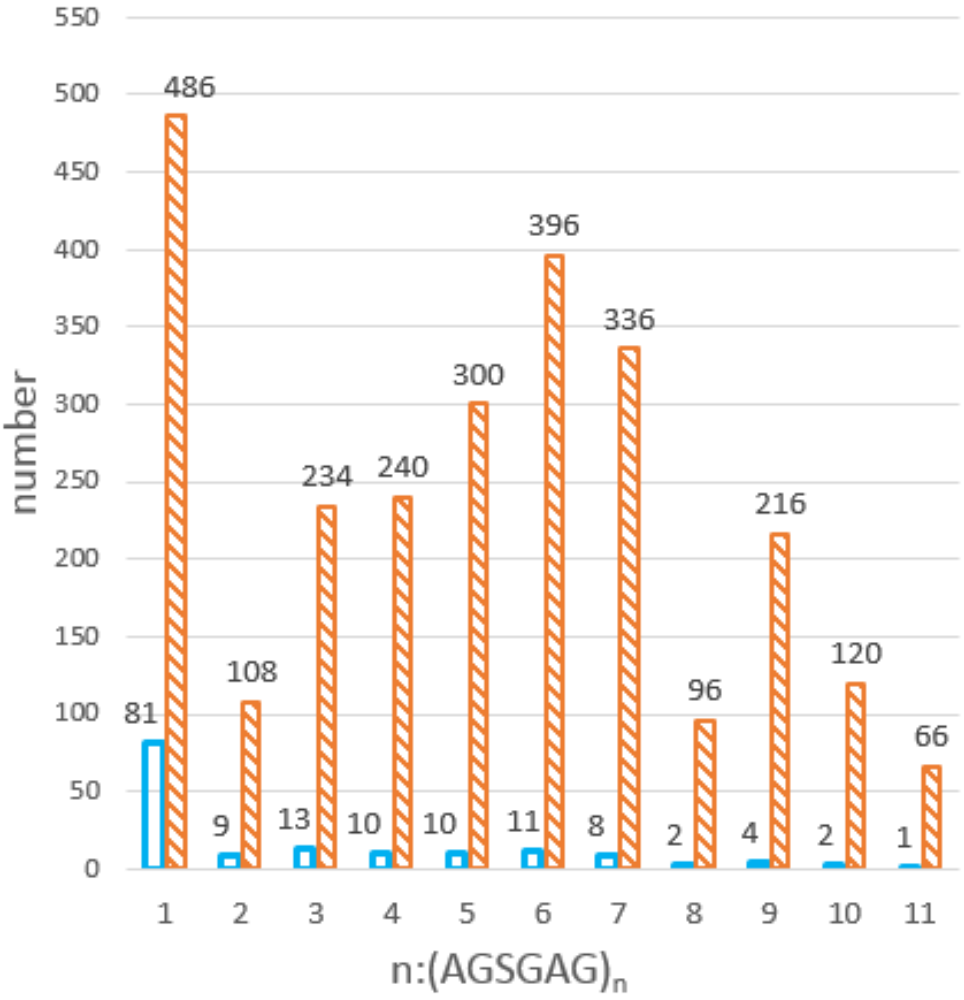

Figure 1. Histograms of the number of occurrences of each $(AGSGAG)_n$ sequence for n=1-11 (blue), and total numbers of amino acid residues of each $(AGSGAG)_n$ in the primary structure of SF heavy chain (orange stripes)[14].

amorphous regions. The properties of SF originate basically from the combination of these unique amino acid sequences, translating them into higher order structures.

Two distinct structures of SF in the solid state have been reported: Silk I as the solid-state SF structure stored in the middle silk glands after drying without any external forces, and Silk II as the structure after spinning [15]. The main conformation of Silk I,

Silk I*, has been determined to be a repeated type II β-turn using stable-isotope labeled SF and the model peptide $(AG)_{15}$ as a structural model for the typical sequence of the crystalline domain of SF, and using mainly several solid-state NMR techniques [16-19]. On the other hand, the structure of Silk II was first characterized by Marsh, Corey, and Pauling [20] using fiber diffraction as a regular array of antiparallel (AP) β-sheets, which remains the classic image of β-sheet silk. Later, Fraser et al. [21], Lotz and Keith [15], Fossey et al. [22] and Takahashi et al. [23] supported the general features of this AP β-sheet model, but some of them also pointed out the presence of intrinsic structural disorder in the Silk II structure based on the X-ray diffraction studies. There are no further reports about SF in Silk II form at atomic level using X-ray fiber diffraction analysis since 1999 [23].

We have studied Silk II structure using several kinds of solid-state NMR and the appropriate model peptides coupled with selective stable isotope labeling [19, 24-37]. Especially, the methyl side chains of the Ala residues are located outside of the backbone of SF and are therefore sensitive to the packing of the amino acid residues of SF chains. Figure S2 shows the Ala Cβ peaks of the ^{13}C cross polarization/ magic angle spinning (CP/MAS) spectra of (a) native SF fiber, (b) the Cp fraction in Silk II form, i.e., precipitated fraction after chymotrypsin cleavage of SF [38], and (c) their difference (a) – (b) [25-29]. The spectrum of the Cp fraction was deconvoluted into three peaks, **t** (32%), **A** (45%) and **B** (23%). The peak **t** was assigned to random coil and/or distorted β-turn, while the other two peaks were assigned to **A** (19.5 ppm) and **B** (22.1 ppm) in both AP β-sheet structures [37]. Two broad peaks were obtained in the spectrum (c) and could be reproduced well by the observed Ala Cβ spectra of the model peptides, for example, Tyr containing model peptides such as (d) $(AGYGAG)_5$, (e)

$(AGAGYGAGAG)_3$ and $(AG)_3YGAGVGAGYG(AG)_3YG(AG)_3$ which are typical sequences in the non-crystalline domain of SF [26-28].

Most recently, we proposed a lamellar structure for the crystalline domain of SF fiber based on structural analyses of the Ala Cβ peaks in the ^{13}C CP/MAS NMR spectra of $(AG)_m$ (m = 9, 12, 15 and 25) and a series of ^{13}C selectively labeled $(AG)_{15}$ model peptides [37]. Hereafter, several excellent physical properties of SF fiber including the application to biomaterials should be studied by taking into account the lamellar structure for the crystalline domain of SF. Thus, the proposal of the lamellar structure seems very important.

In this paper, we expanded our solid-state NMR study to a better mimic than $(AG)_m$, i.e., a series of $(AGSGAG)_n$ (n=2-5 and 8) (Figure 1) of the Cp fraction. In addition, ten kinds of [3-^{13}C]Ala-$(AGSGAG)_5$ peptides synthesized previously [33] were used again. Moreover, the dynamics of the Ala Cβ carbons in the different environments of the Cp fraction and their model peptides, [3-^{13}C]Ala-$(AGSGAG)_5$ were studied in detail by the determination of ^{13}C solid-state spin-lattice relaxation time (T_1) values for the three components of the Ala $^{13}C\beta$ peaks [39-41].

2. Materials and methods

2.1. Sample Preparation

We used the peptides $(AGSGAG)_n$ where n = 2, 3, 4, 5 and 8. A fully automated Pioneer Peptide Synthesis System (Applied Biosystem Ltd.) [16-18, 26-34] was used throughout. The peptides, n = 5 and 8 were already prepared in our laboratory [32,33] and other peptides, n = 2,3 and 4 were synthesized here. The Cp fraction with Silk II

form prepared previously [34,36] was also used. Ten [3-^{13}C]Ala-(AGSGAG)$_5$ peptides with different ^{13}C labeling positions synthesized previously [33,34] were used to determine the fractions of several conformations of Ala residues by deconvolution of the [3-^{13}C]Ala peaks. Eight of the peptides were also used to determine the T_1 values of the three components of the Ala peaks. These peptides were precipitated after dialysis of 9M LiBr solution against distilled water and took Silk II form, and were used for a series of ^{13}C solid-state NMR studies.

2.2. ^{13}C solid-state NMR measurements

A Bruker AVANCE 400 NMR spectrometer was used for recording the ^{13}C CP/MAS NMR spectra of the samples. A ^{1}H 90° pulse of 3.0 μs, a ramped CP pulse with a contact time of 2 ms, and a TPPM ^{1}H decoupling pulse with an amplitude of 70 kHz during acquisition were used according to previous papers [34,36]. A total of 256 (for ^{13}C labeled samples) and 2,048 (for non-labeled samples) scans were collected. Lorentzian line broadening of 20 Hz was applied prior to Fourier transformation. The fractions of three components of the Ala Cβ peaks were determined after a peak deconvolution analysis based on a Gaussian line-shape. The half-height-widths were changed after fixing the chemical shifts [31-33, 37]. The ^{13}C chemical shifts were calibrated externally using the methylene peak of adamantane at 28.8 ppm from an external reference of tetramethylsilane (0 ppm). The ^{13}C T_1 values of three components of the Ala Cβ peaks of the Cp fraction and eight kinds of [3-^{13}C]Ala-(AGSGAG)$_5$ peptides were determined using the method reported by Torchia [42] with delay times from 0 to 1,000 ms at 25°C. The T_1 values were also observed at 40°C and 60°C to determine temperature dependences of the T_1 values for three components of the Ala Cβ peaks of the Cp

fraction and [3-^{13}C]Ala^{19}-(AGSGAG)$_5$. Then the correlation times of the hopping motion of Cβ carbon about the C_3 axis of the Ala residue under MAS condition were determined from the temperature-dependent T_1 values.

3. Results

3.1. Determination of the fractions of the three Ala Cβ peaks of (AGSGAG)$_n$ (n=2-5 and 8).

The ^{13}C CP/MAS NMR spectra of (AGSGAG)$_5$ and the Cp fraction are shown in Figure 2. The chemical shifts of all main peaks, i.e., Ala Cα, Ala Cβ, Ala C=O, Ser Cα, Ser Cβ, Ser C=O, Gly Cα and Gly C=O peaks, were very similar between both samples, indicating that these samples took basically the same conformations, namely an antiparallel (AP) β-sheet structure [19, 24,29]. Figure 3 shows the expanded Ala Cβ peaks in the ^{13}C CP/MAS NMR spectra of the peptides (AGSGAG)$_n$ (n = 2-5 and 8) and the Cp fraction. The line shapes of (AGSGAG)$_n$ (n = 2 and 3) are similar. The shoulder peak at higher field was assigned to random coil and the main peak at lower field to AP β-sheet structure [19, 25-29]. On the other hand, the line shapes were different from those of (AGSGAG)$_n$ (n = 4, 5 and 8) and the Cp fraction. Namely, the main peaks at 19.5 ppm became sharper and had a shoulder at lower field, 21.8 ppm. Thus, the Ala Cβ peaks of (AGSGAG)$_n$ (n = 4,5 and 8) and the Cp fraction can be deconvoluted to three peaks named **t** (distorted β-turn), **A** (AP-β sheet) and **B** (AP-β sheet) from higher to lower field as shown in Figure 4. The chemical shifts and half-

height-widths used in the peak deconvolutions to determine the fractions of three components are listed in Table S1. The relative percentages of each were 23.3-24.0 for the peak **B** at 21.8 ppm, 44.0-45.4 for the 19.5 ppm peak **A**, and 30.9-32.7 for the 16.5 ppm peak **t**, and thus the fractions of the peaks, **t, A** and **B** were almost the same among these four samples. Thus, $(AGSGAG)_4$ is considered to be the minimum length to form a structure similar to that of the Cp fraction. We used $(AGSGAG)_5$ as the model of the Cp fraction [33,34] for the detailed discussion below.

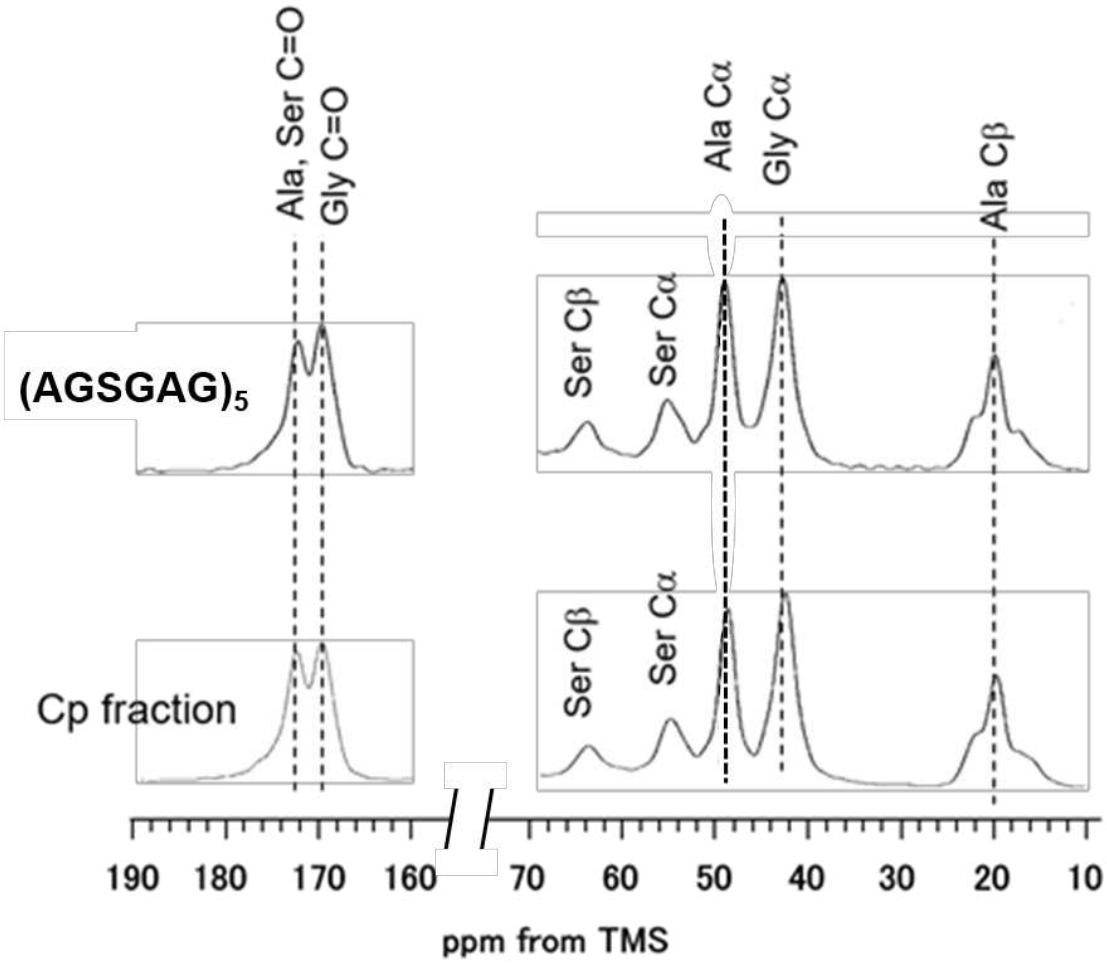

Figure 2. ^{13}C CP/MAS NMR spectra of $(AGSGAG)_5$ and Cp fraction in the Silk II forms of SF together with their assignments [24,27].

.

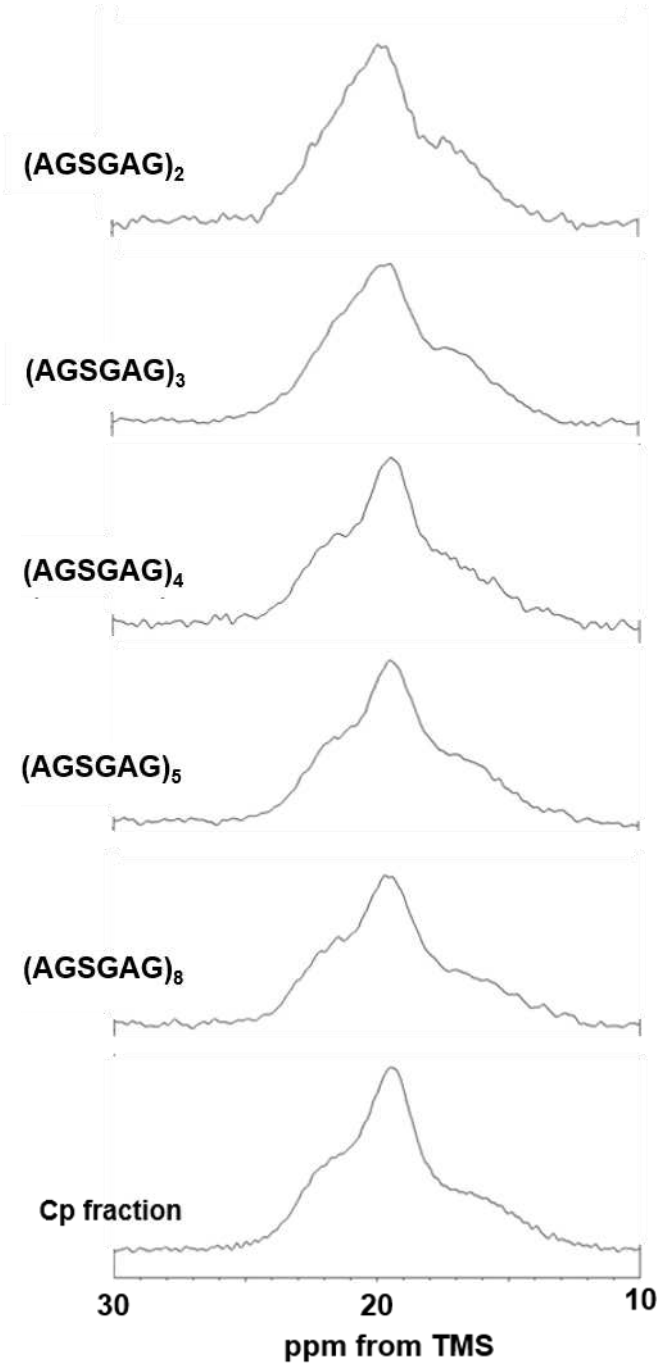

Figure 3. Expanded Ala Cβ peaks in the ^{13}C CP/MAS NMR spectra of $(AGSGAG)_n$ (n = 2,3,4,5 and 8) and Cp fraction in the Silk II forms.

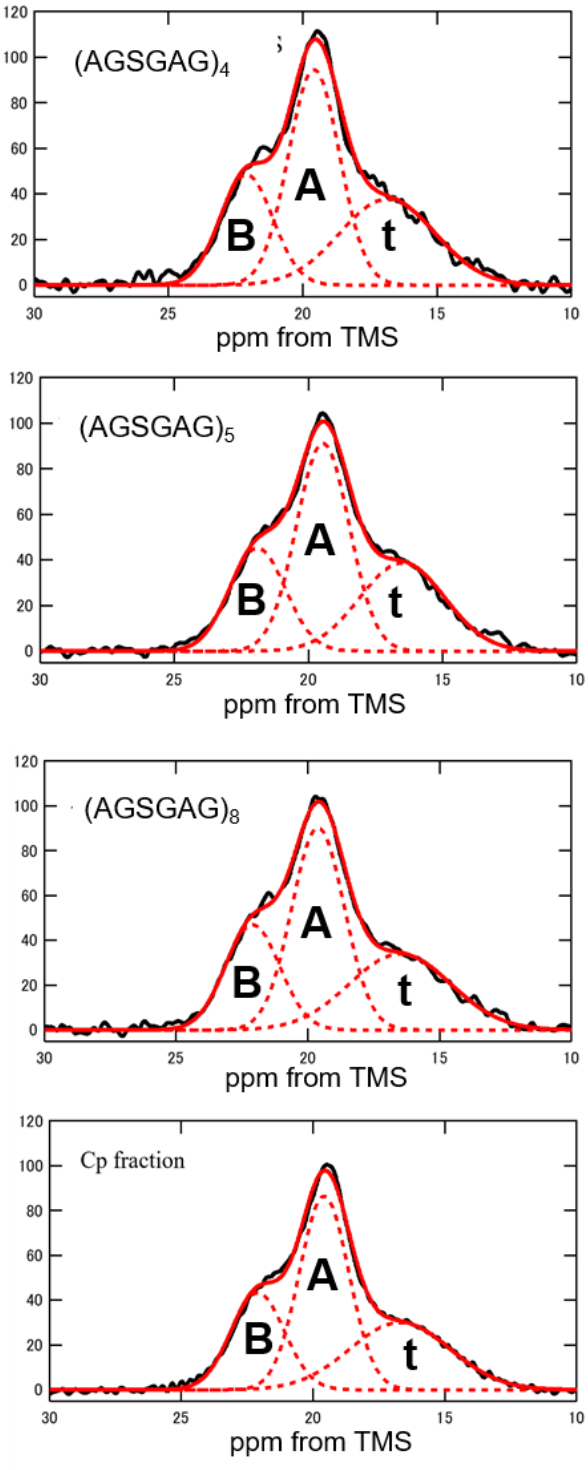

Figure 4. The three deconvoluted Ala Cβ peaks, i.e., **t** (random coil), **A** (AP-β sheet) and **B** (AP-β sheet) of $(AGSGAG)_n$ (n = 4,5 and 8) and Cp fraction.

3.2. Lamellar structure of (AGSGAG)$_5$ proposed by the determination of the fractions of three components in the Ala Cβ peaks of (AGSGAG)$_5$

Figure 5 shows the expanded ^{13}C Ala Cβ peaks in the ^{13}C CP/MAS NMR spectra of ten kinds of [3-^{13}C]Ala-(AGSGAG)$_5$ peptides with different [3-^{13}C]Ala labeling positions together with their deconvolution. The assignment of the three deconvoluted peaks is **B**, **A** and **t** from low to high field as marked in Figure 4 except for Ala-01 where the peak **B** could not be observed. The fractions together with the deconvolution parameters, i.e., the chemical shift and half-height-width are listed in Table 1. The half-height-width tends to be larger in the order **A**, **B** and **t**. The fractions of the three Ala Cβ peaks are plotted against the ^{13}C labeled position for [3-^{13}C]Ala-(AGSGAG)$_5$ peptides in Figure 6. Those of the fifteen kinds of [3-^{13}C]Ala-(AG)$_{15}$ reported previously [29,32,37] are shown in Figure S3. At first, we discuss changes in the fraction of the peak **t** in Figure 6. At position 1, the fraction was 83.5% after which it decreased rapidly, with maxima at positions 11, 19 and 29. The fractions of the peaks **A** and **B** assigned to AP β-sheet tend to change inversely with the change of the fraction of the peak **t** and there are minima at positions 11 and 19. The decrease in peak **t** at positions 5 to 7, and 23 to 25, and conversely the increase in peak **A**, is striking, and indicates that these regions tend to form AP β-sheet rather than random coil.

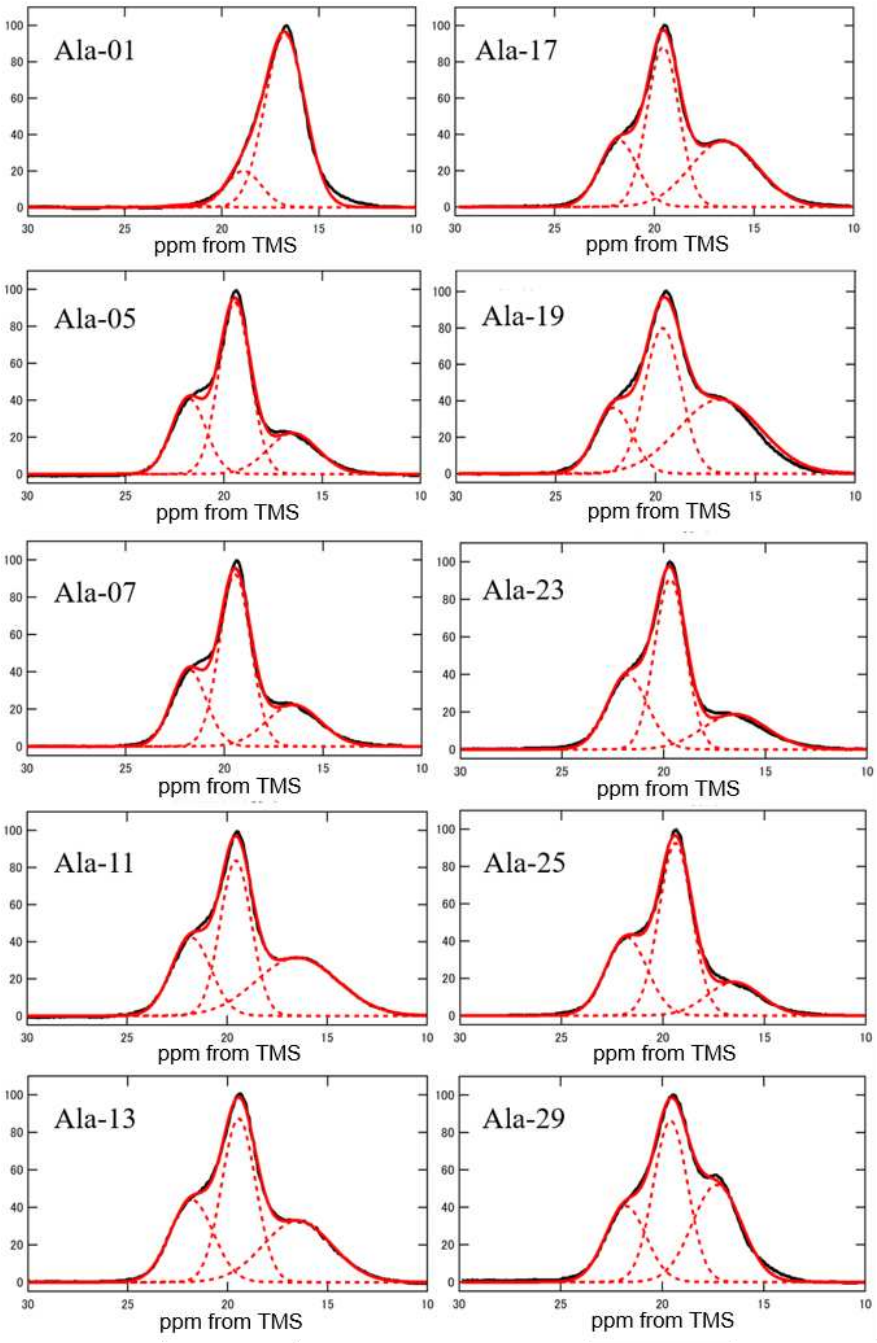

Figure 5. Deconvoluted ^{13}C-labeled Ala Cβ peaks in the ^{13}C CP/MAS NMR spectra of ten kinds of [3-^{13}C]Ala-(AGSGAG)$_5$ peptides with different ^{13}C labeling positions.

Table 1. The ^{13}C chemical shift (in ppm), half-height-width (Hz) and fraction obtained from the deconvolutions of the Ala Cβ peaks of ten kinds of [3-^{13}C]Ala-(AGSGAG)$_5$.

^{13}C-labeled position		Chemical shift (ppm)	Half-height-width (Hz)	Percentage
Ala-01	**B**	—	—	—
	A	18.9	216	16.5
	t	16.8	242	83.5
Ala-05	**B**	21.8	206	25.9
	A	19.5	188	53.7
	t	16.5	300	20.4
Ala-07	**B**	21.8	208	26.0
	A	19.5	186	52.3
	t	16.5	322	21.7
Ala-11	**B**	21.8	232	24.4
	A	19.6	184	38.3
	t	16.5	478	37.2
Ala-13	**B**	21.8	252	26.5
	A	19.4	200	41.8
	t	16.5	406	31.7
Ala-17	**B**	21.8	224	20.9
	A	19.6	188	42.2
	t	16.5	400	36.8
Ala-19	**B**	22.1	218	17.7
	A	19.6	214	38.3
	t	16.7	486	44.0
Ala-23	**B**	21.8	236	28.6

	A	19.7	180	50.1
	t	16.5	372	21.4
Ala-25	**B**	21.8	240	30.1
	A	19.4	192	53.2
	t	16.5	312	16.7
Ala-29	**B**	21.8	236	23.1
	A	19.6	200	41.4
	t	17.3	284	35.6

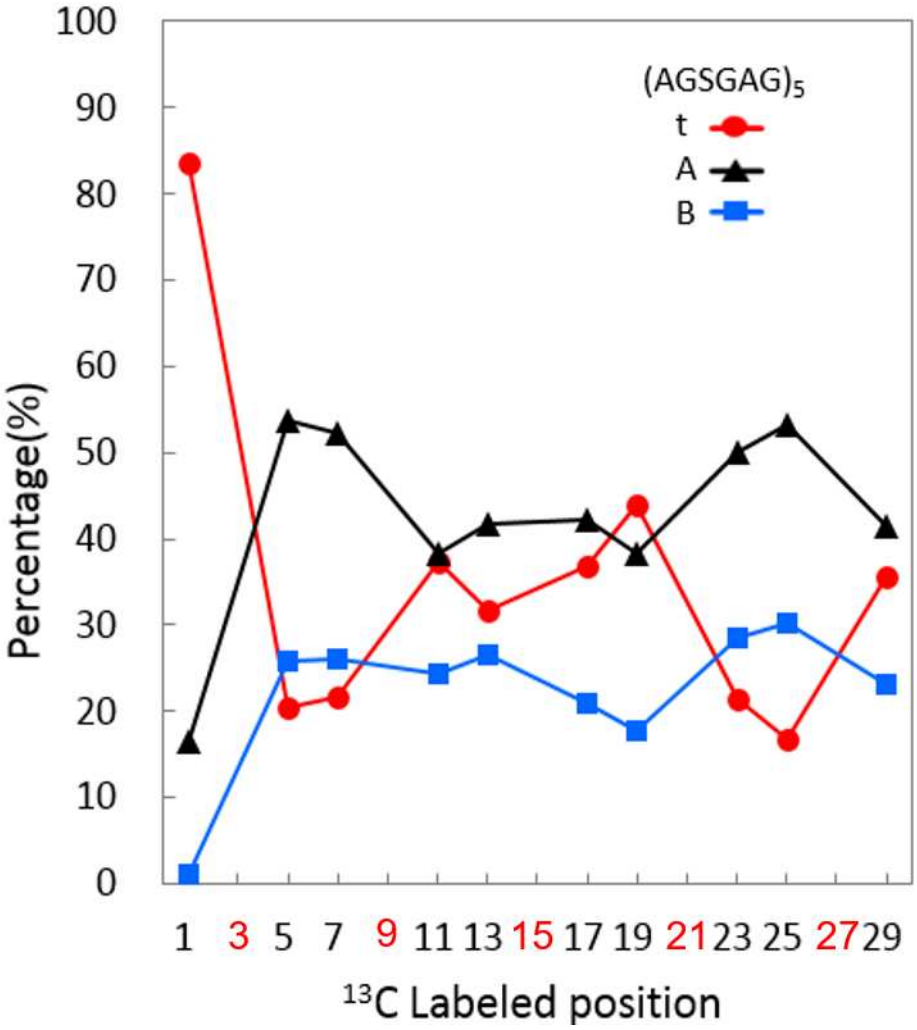

Figure 6. Changes in the percentages of peaks **t**, **A** and **B** of ^{13}C-labeled Ala Cβ carbon of ten kinds of [3-^{13}C]Ala-(AGSGAG)$_5$ peptides plotted as a function of the ^{13}C labeled position. The positions 3, 9, 15, 21 and 27 (red) in [3-^{13}C]Ala-(AGSGAG)$_5$ are Ser residues, not Ala residues. The deconvoluted Ala Cβ peaks are shown in Figure 5 and the fractions together with the deconvolution parameters, the chemical shift and half-height-width are summarized in Table S2. The plots of the fractions of three peaks, **t**, **A** and **B** of ^{13}C-labeled Ala Cβ peaks of fifteen kinds of [3-^{13}C]Ala-(AG)$_{15}$ peptides are also shown in Figure S3 for comparison.

This pattern suggests a lamellar structure of (AGSGAG)$_5$ with a repetitive folding predominantly through turns at positions 11 and 19, i.e. every eighth amino acid, as

shown in Figure 7. This structure generates three types of alanine (**t**, **A**, **B**) in a ratio 1:2:1, in which **t** is in a turn, **A** is in an antiparallel β-sheet, i.e., Ala residue with **A** structure is located at a position where both sides are Gly residues in β-sheet, and **B** is also in an AP β-sheet, i.e., Ala residue with **B** structure is located at the position where one side is a Gly residue in β-sheet and the other side is a Gly residue in β-turn, and thus **B** structure is a less sterically restricted environment. If the lamellar structure has turns exclusively at the positions 11 and 19, the fractions of the peaks **t** at these positions should be 100%. However, the fractions were 37.2 % and 44.0 %, respectively. To examine these fractions, we consider eight possible lamellar structures (I)-(VIII) with repetitive folding through turns every eighth amino acid, changing the turn position systematically as shown in Figure 8. For example, when we consider the position 11 marked by the circle, the Ala^{11} residue takes **t** structure in (I) and (V). Then, in (II), (III), (VI) and (VII), the Ala^{11} residue takes **A** structures. In (IV) and (VIII), the Ala^{11} residue takes **B** structure. If the structures (I) to (VIII) appeared with the same probability, the fraction of the structures (I) and (V) should be 25% and therefore the fraction of **t** at position 11 should be 25%. However, the observed fraction at 37.2% is considerably larger than 25%. Similarly, the fraction of **t** at position 19 is 44.0%, which is also considerably larger than 25%. Therefore, we propose a lamellar structure of $(AGSGAG)_5$ with a repetitive folding predominantly through turns at positions 11 and 19 as shown in Figure 7, such that (I) and (V) (Figure 8) have significantly higher population. In our previous paper discussing [3-^{13}C]Ala-$(AG)_{15}$ [37], it was concluded that two lamellar molecules formed head-to-tail binding through inter-molecular hydrogen bond formation between NH_3^+ in the Ala^1 residue of one molecule and CO_2^- in the Gly^{30} residue of another molecule, based on REDOR

experiments. Here, two $(AGSGAG)_5$ molecules are also suggested to form head-to-tail binding through inter-molecular hydrogen bond formation.

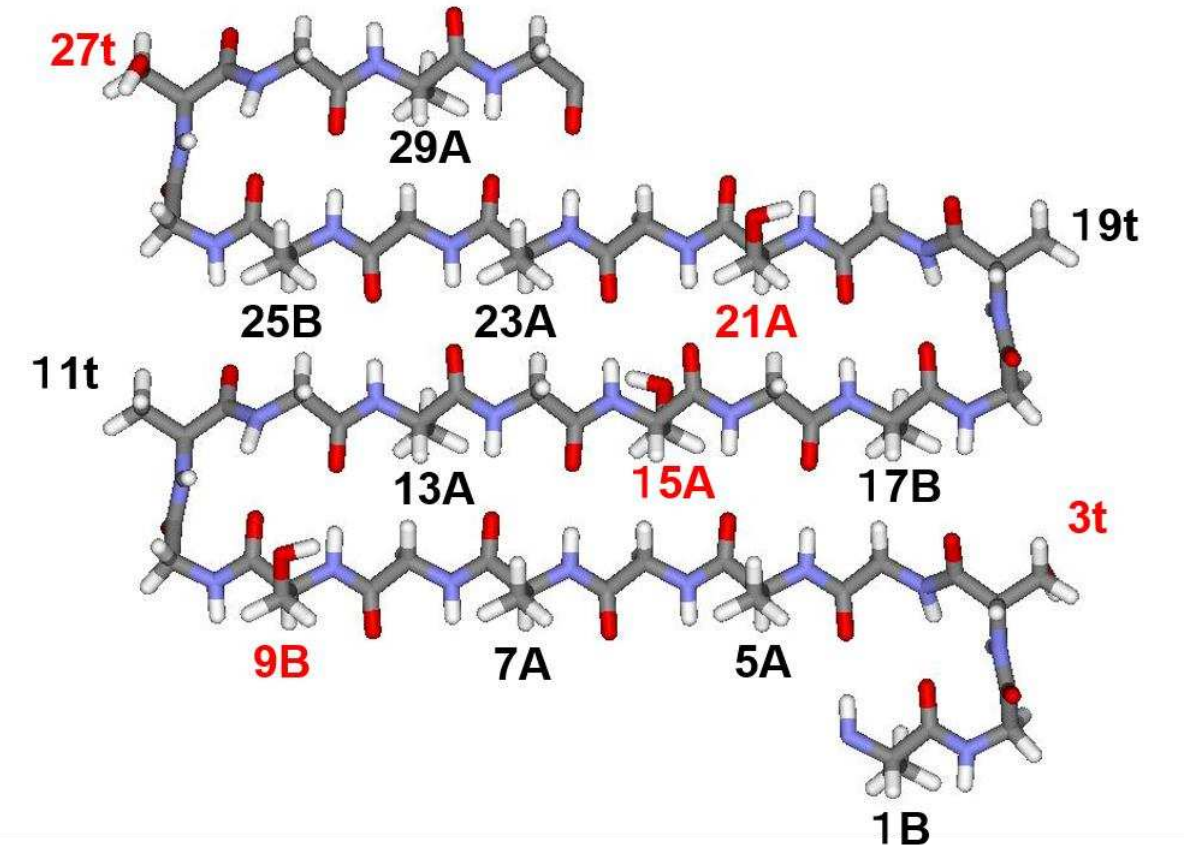

Figure 7. Lamellar structure of $(AGSGAG)_5$ in an antipolar arrangement with β-turns at the positions 11 and 19, formed by repetitive folding using β-turns every eighth amino acid. Three peaks, **t**, **A** and **B** in the ^{13}C-labeled Ala Cβ peak can be assigned to three kinds of Ala Cβ carbons (black letters). The difference between **A** and **B** is that **B** is at the end of the β-strand and is in a less restricted environment. The red letters indicate the Ser Cβ carbons in $(AGSGAG)_5$ corresponding to the Ala Cβ carbons in $(AG)_{15}$ lamellar structure. The side chain conformations of the Ser Cα-Cβ bonds were assumed to be *gauche*+ [43].

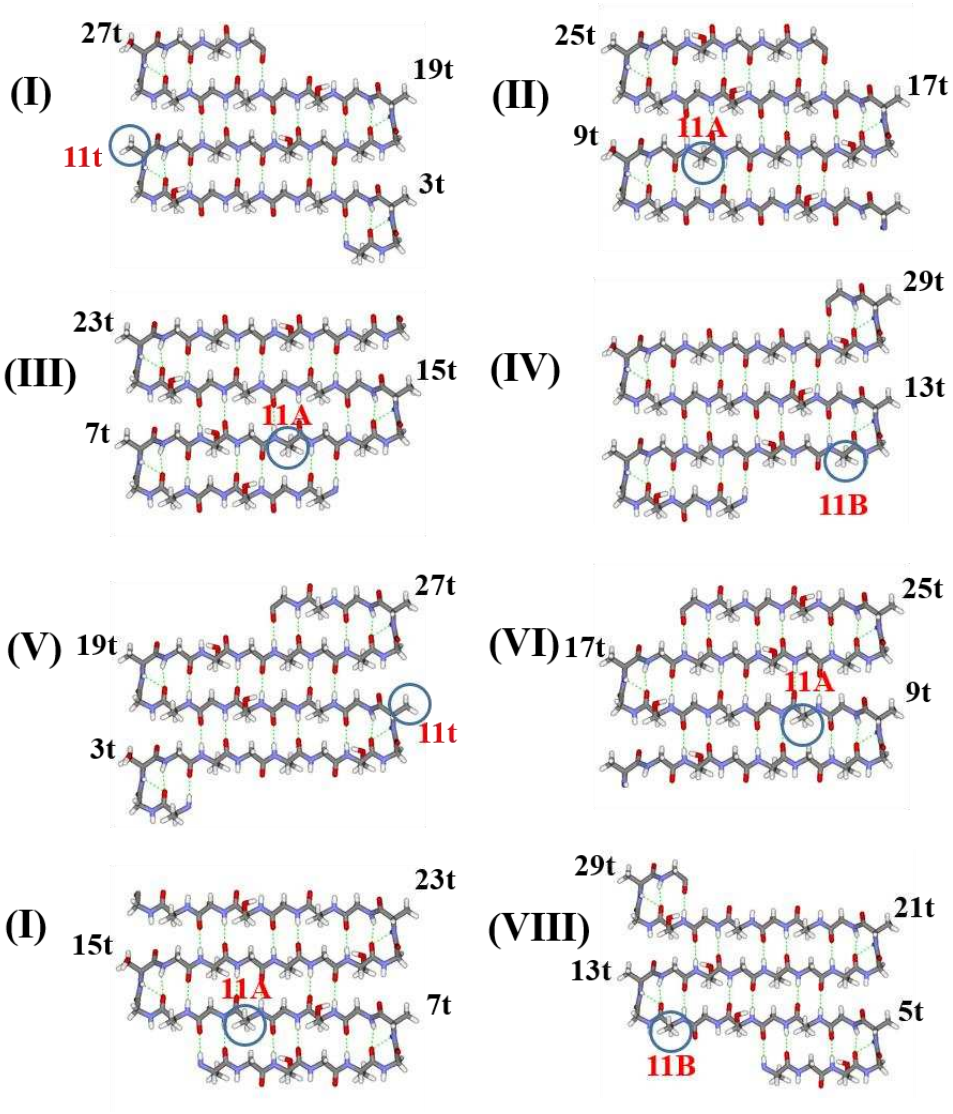

Figure 8. Eight possible lamellar structures, (I)-(VIII), formed by repetitive folding through turns every eighth amino acid and antipolar stacking. The positions of the β-turns were assigned numerical values and the position of Ala-11 is circled. The side chain conformations of the Ser Cα-Cβ bonds were assumed to be *gauche*+ [43].

As a whole, the changes in the fractions of the three peaks as a function of ^{13}C labeling position in [3-^{13}C] Ala-(AGSGAG)$_5$ (solid lines) have a similar tendency to those in [3-

^{13}C] Ala-$(AG)_{15}$ (broken lines) (Figure S3), although the absolute values of the fractions of the peak **t** increased and those of the peak **A** decreased for [3-^{13}C] Ala-$(AGSGAG)_5$ compared with those of [3-^{13}C] Ala-$(AG)_{15}$ [37]. The absolute values of the fractions of the peak **B** including their changes as a function of ^{13}C labeling position are almost the same between the two kinds of peptides. Thus, it is interesting that the lamellar structure is essentially the same as that of $(AG)_{15}$ although the side chain at the positions of 3, 9, 15, 21 and 27 in the chain is changed from CH_3 to CH_2OH and therefore hydrogen bonds through the side chain OH groups are expected to occur in $(AGSGAG)_5$ [33,34,43-46]. In order to examine differences in the lamellar structures between $(AG)_{15}$ and $(AGSGAG)_5$ in view of the dynamics of both samples in Silk II form, the ^{13}C T_1 values of [3-^{13}C]Ala-$(AGSGAG)_5$ were observed and compared with those of [3-^{13}C]Ala-$(AG)_{15}$ at the same ^{13}C labeling positions.

3.3. Temperature Dependences of the ^{13}C solid-state spin-lattice relaxation times of Ala Cβ carbons in the Cp fraction and [3-^{13}C]Ala^{19}-$(AGSGAG)_5$

Figure 9(a) shows a series of partially relaxed Ala Cβ peaks in the ^{13}C CP/MAS NMR spectra of the Cp fraction and [3-^{13}C]Ala^{19}-$(AGSGAG)_5$ as an example at 25°C. It is clear that the T_1 values of the peaks **B** at the lowest field are the longest in both samples. The log plots of the intensities of the three partially relaxed Ala Cβ peaks, **t**, **A** and **B** versus delay time τ are shown in Figure 9 (b). The log plots changed linearly for both samples, implying a single component of motion about the Ala Cβ side chain motion for the Cp fraction and [3-^{13}C]Ala^{19}-$(AGSGAG)_5$.

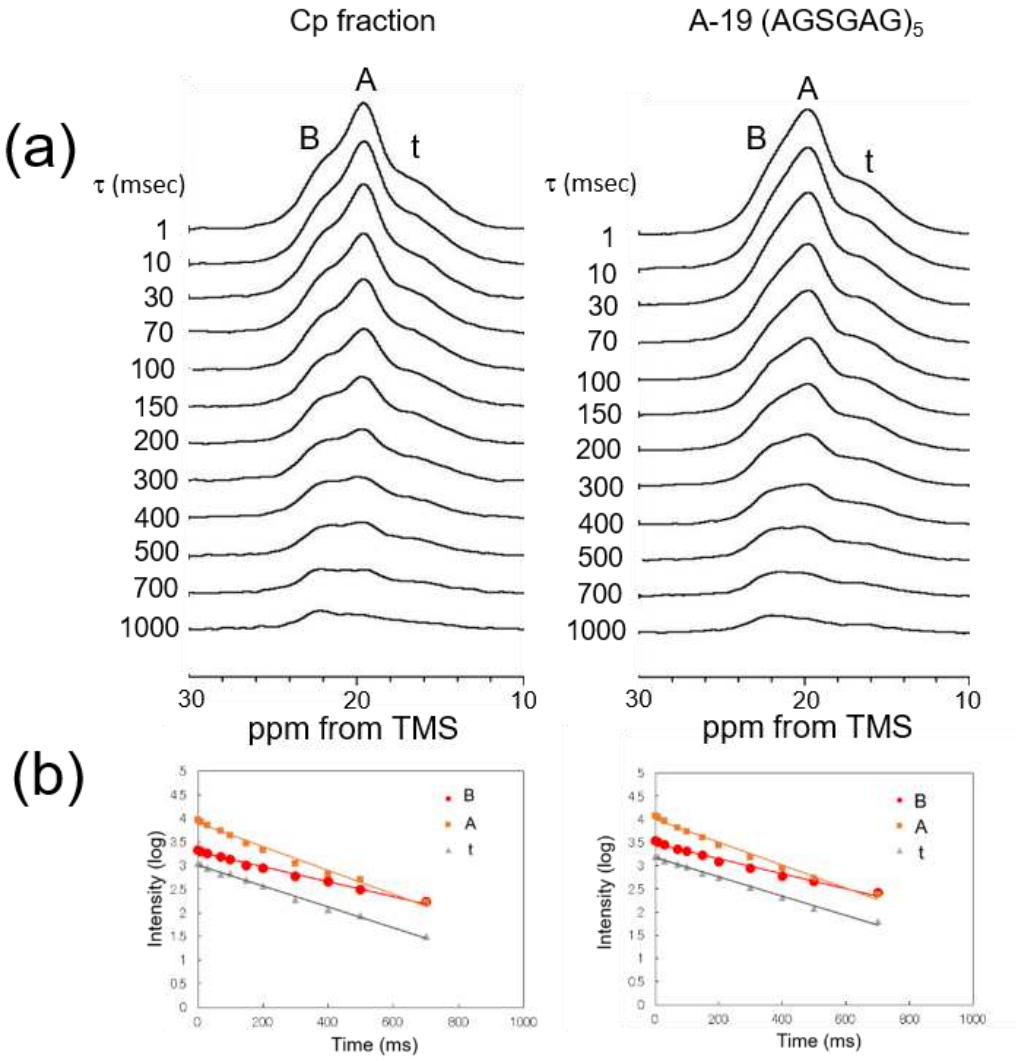

Figure 9 (a) A series of partially relaxed Ala Cβ peaks in the ^{13}C CP/MAS NMR spectra of Cp fraction and [3-^{13}C]Ala^{19}-$(AGSGAG)_5$ at 25°C. (b) Observed plots of the log intensities of partially relaxed Ala Cβ peaks vs delay time (ms) for Cp fraction and [3-^{13}C]Ala^{19}-$(AGSGAG)_5$.

In the case of Ala Cβ, its ^{13}C spin lattice relaxation in solid state is well characterized using three-site hopping motion, and ^{13}C T_1 values for Ala Cβ under MAS condition are explicitly expressed as follows [47].

$$\frac{1}{T_1^C} = \frac{\gamma_C^2 \gamma_H^2 \hbar^2 I(I+1)}{r^6}\left[\frac{1}{12}J^{(0)}(\omega_C - \omega_H) + \frac{3}{2}J^{(1)}(\omega_C) + \frac{3}{4}J^{(2)}(\omega_C + \omega_H)\right] \qquad (1)$$

where,

$$J^{(0)}(\omega) = \frac{6}{5}(sin^2 2\Delta + sin^4\Delta)\left[\frac{t_c}{1+\omega^2\tau_c^2}\right]$$

$$J^{(1)}(\omega) = \frac{1}{5}(sin^2 2\Delta + sin^4\Delta)\left[\frac{tc}{1+\omega^2\tau_c^2}\right]$$

$$J^{(2)}(\omega) = \frac{4}{5}(sin^2 2\Delta + sin^4\Delta)\left[\frac{tc}{1+\omega^2\tau_c^2}\right],$$

where, I is the spin quantum number of proton (½), ω_C and ω_H are Larmor angular frequencies of carbon and proton nuclei, respectively, Δ is the angle between the C-H internuclear vector and the C_3 axis, and τ_c is the correlation time of the hopping motion of methyl groups about the C_3 axis. Using this equation and parameters of the anisotropic motion of methyl group (Δ = 69.8º, r_{CH}=1.098 Å in L-alanine crystal [48]), ^{13}C T_1 values can be evaluated using the experimentally obtained ^{13}C T_1 value and its temperature dependence. Aa series of partially relaxed Ala Cβ spectra of both samples were observed with increasing temperature, in order to measure the T_1 values of the Ala Cβ carbons of the Cp fraction and [3-^{13}C]Ala^{19}-(AGSGAG)$_5$, and to determine whether they are located at the shorter or longer τ_c region from the value at the T_1 minimum in the plot of T_1 values against the 1/T (K^{-1}) values, and to determine the correlation time τ_c of the Ala Cβ side chain motion for the Cp fraction and [3-^{13}C]Ala^{19}-(AGSGAG)$_5$ using Eq. 1. The T_1 values of the Ala Cβ peaks determined at 25°C, 40°C and 60°C are listed in Table 2 together with the fitted correlation times. With increasing temperature, all T_1 values of the three Ala Cβ peaks, **B**, **A** and **t** increased,

indicating these values are located at the shorter τ_c region from the value at the T_1 minimum in the plot of T_1 values against the 1/T values. Thus, a longer T_1 value of the Ala Cβ peak in the samples used here means faster motion. The correlation times increase in the order **B**, **t** and **A**, with **B** having considerably faster motion than the other two.

Table 2. The ^{13}C solid-state spin-lattice relation times (T_1: msec) and correlation times (τ_c: $\times 10^{-11}$s) of the Cp fraction and [3-^{13}C]Ala^{19}- (AGSGAG)$_5$ at 25°C, 40°C and 60°C.

Sample		T_1 (msec)		
		25 ºC	40 ºC	60 ºC
Cp fraction	**B**	643±19	706±30	734±23
	A	406±16	433±17	451±15
	t	453±13	532±24	540±18
			τ_c ($\times 10^{-11}$ s)	
	B	2.8	2.3	2.2
	A	4.2	4.1	3.9
	t	3.9	3.3	3.3
			T_1 (msec)	
[3-^{13}C]Ala^{19}-(AGSGAG)$_5$	**B**	625±27	633±17	689±16
	A	409±16	422±15	451±16
	t	485±14	489±20	525±19
			τ_c ($\times 10^{-11}$ s)	
	B	2.8	2.8	2.5
	A	4.2	4.1	4.0
	t	3.7	3.7	3.3

3.4. ^{13}C solid-state spin-lattice relaxation times of the Ala Cβ carbons in [3-^{13}C]Ala-(AGSGAG)$_5$ with different ^{13}C labeling positions and comparison with those in [3-

^{13}C]Ala-(AG)$_{15}$ with the same ^{13}C labeling positions.

Although the side chain at positions 3, 9, 15, 21 and 27 in the chain changed from CH_3 in $(AG)_{15}$ to CH_2OH in $(AGSGAG)_5$, we propose a similar lamellar structure for $(AGSGAG)_5$ as for $(AG)_{15}$: both lamellar structures are formed by repetitive folding using β-turns every eighth amino acid in antipolar arrangement. Using solid-state NMR data, we have previously shown that the Ser sidechain OH groups in the Cp fraction and $(AGSGAG)_5$ form hydrogen bonds [33,34,43-46], so we investigated the effect of Ser OH hydrogen bonding on dynamics by investigating the ^{13}C T_1 values of the Ala Cβ carbons in [3-^{13}C]Ala-$(AGSGAG)_5$ with different ^{13}C labeling positions. The ^{13}C T_1 values determined for eight kinds of [3-^{13}C]Ala-$(AGSGAG)_5$ with different ^{13}C labeling positions are listed in Table 3 together with the ^{13}C T_1 values of the eight kinds of [3-^{13}C]Ala-$(AG)_{15}$ with the same ^{13}C labeling positions for a comparison. Figure 10 shows changes in the ^{13}C T_1 values of three Ala Cβ peaks, **t**, **A** and **B** of [3-^{13}C]Ala-$(AGSGAG)_5$ as a function of the ^{13}C labeling position (solid lines) and those of [3-^{13}C]Ala-$(AG)_{15}$ for a comparison (broken lines).

Table 3. The ^{13}C solid-state spin-lattice relation times of ^{13}C Ala Cβ peaks, **t**, **A** and **B** of [3-^{13}C]Ala-$(AGAGAG)_5$ and [3-^{13}C]Ala-$(AG)_{15}$ at 25 ºC

^{13}C-position			T_1(msec) at 25 ºC		
			$(AGSGAG)_5$		$(AG)_{15}$
Ala-01	**B**	■	-	□	1158±104
	A	▲	508±13	Δ	427±10
	t	●	559±11	○	456±7
Ala-05	**B**	■	694±28	□	872±40
	A	▲	366±14	Δ	372±9
	t	●	436±92	○	450±8
Ala-07	**B**	■	675±31	□	827±44
	A	▲	350±12	Δ	354±9
	t	●	446±11	○	417±7
Ala-11	**B**	■	660±27	□	858±41
	A	▲	363±20	Δ	389±12
	t	●	439±22	○	503±14
Ala-13	**B**	■	644±34	□	820±35
	A	▲	367±11	Δ	369±11
	t	●	463±16	○	432±32
Ala-19	**B**	■	625±27	□	897±100
	A	▲	409±16	Δ	407±16
	t	●	485±14	○	473±17
Ala-23	**B**	■	693±34	□	823±21
	A	▲	370±12	Δ	378±8
	t	●	460±15	○	457±12
Ala-29	**B**	■	590±29	□	1080±78
	A	▲	380±14	Δ	460±13
	t	●	488±14	○	636±34

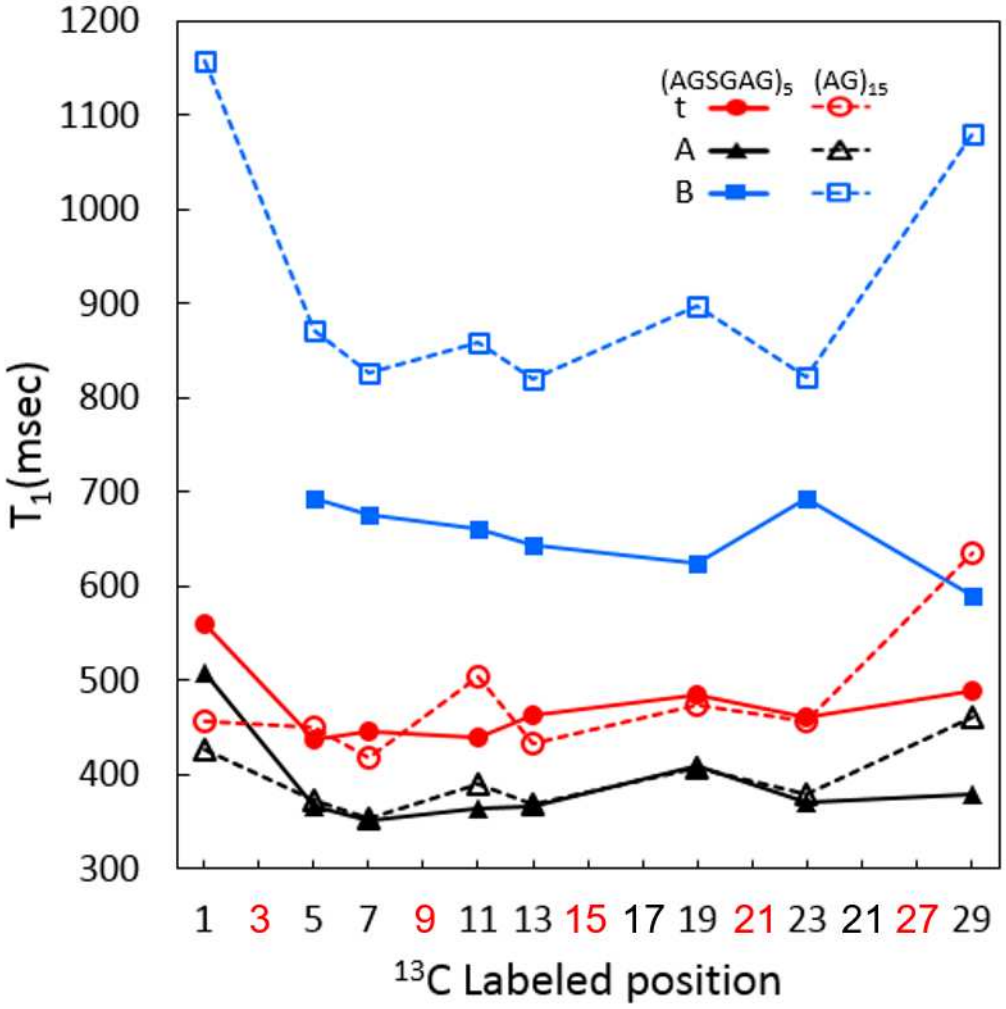

Figure 10 Changes in the T_1 values of peaks **t**, **A** and **B** of ^{13}C-labeled Ala Cβ carbons of eight kinds of [3-^{13}C]Ala-(AGSGAG)$_5$ peptides plotted as a function of the ^{13}C labeled position (broken lines). The positions 3, 9, 15, 21 and 27 (red) in [3-^{13}C]Ala-(AGSGAG)$_5$ are Ser residues, not Ala residues. The deconvoluted Ala Cβ peaks are shown in Figure 5 and the fractions are summarized in Table 2. The plots of the T_1 values of peaks **t**, **A** and **B** of ^{13}C-labeled Ala Cβ carbons of eight kinds of [3-^{13}C]Ala-(AG)$_{15}$ peptides are also shown as solid lines for a comparison.

The T_1 values of [3-^{13}C]Ala-$(AGSGAG)_5$ are reasonably independent of position in the chain, with the exception of the termini, which have longer T_1 as expected. They increase in the order **A** < **t** < **B** for all ^{13}C labeled positions, indicating that methyl group rotation for methyls **B** in lamellar $(AGSGAG)_5$ is faster than for **A** and **t**. The most striking difference in T_1 values between [3-^{13}C]Ala-$(AGSGAG)_5$ and [3-^{13}C]Ala-$(AG)_{15}$ is that replacement of A by S has resulted in a marked decrease in T_1 for all **B** methyls. We have previously noted [41] that methyls **B** in $(AG)_n$ have much longer T_1 (i.e. much greater rotational freedom) than **A** and **t**, and have suggested that this is because the **B** position, at the end of the β-strand and next to the turn, is less sterically restricted. The observation of significantly shorter T_1 values for **B** methyls in $(AGSGAG)_5$ implies that hydrogen bonding to Ser-OH reduces the rotational mobility of Ala **B** methyls markedly, by increasing the packing density in this region. Inspection of structural models such as Figure 7 suggests that the hydrogen bonds must be from one lamella to its neighbor: the Ser-OH hydrogen bonds serve to fix one lamellar layer against an adjacent one.

4. Discussion

The origin of the high strength of SF fiber is mainly considered to come from the characteristic structure of the crystalline domain of SF. This domain consists of repeated sequences, $(AGSGAG)_n$ (n=1-11) as shown in Figure 1, and therefore peptides are good models for the crystalline domain [13,14]. In our previous paper [37], we proposed a lamellar structure formed by repetitive folding using β-turns every eighth amino acid for the crystalline domain of SF fiber based on structural analyses of the Ala

Cβ peaks in $(AG)_m$ model peptides. In this paper we used $(AGSGAG)_n$, which is a better model, and showed that it forms a very similar lamellar structure. The main difference between them is the presence of Ser-OH hydrogen bonds which lead to tighter interlamellar packing and reduced flexibility in the region of the β-turns.

We have previously characterized the mobility of Ser residues in $(AGSGAG)_n$, which provides more insight into the role of Ser in the lamellar structure. Of the 635 serines in SF, 433 or 68% occur in $(AGSGAG)_n$ repeats, demonstrating the importance of Ser in crystalline SF structure. The side chain conformation around the Ser Cα-Cβ bond when the Ser OH group formed hydrogen bonding was determined using uniaxially aligned [3,3-^{2}H]Ser-SF fiber samples [43]. The ^{2}H solid-state NMR spectral patterns showed that the dominant side chain dihedral angle of the Ser Cα-Cβ bond was the *gauche*+ conformation. Thus, in Figures 7 and 8, the side chain conformations of the Ser Cα-Cβ bonds were assumed to be *gauche*+. The dynamics of the Ser residue has been studied for [3,3-^{2}H]Ser-SF fiber using ^{2}H solid-state NMR [43,45]. Lineshape analyses of the powder patterns showed there are two types of motion about the side chain of the Ser residue. 75% of the Ser residues show a static ^{2}H peak pattern which indicates the formation of hydrogen bonding through the OH group, and 25% of them have a rapid three-site jump motion, indicating no hydrogen bonding formation of the side chain. The ^{13}C T_1s of the Ser Cβ peak in the ^{13}C CP/MAS NMR spectrum of the Cp fraction or [3-^{13}C]Ser-$(AGSGAG)_5$ samples in Silk II forms were also determined [33,34,46]. Two components with shorter and longer T_1 values were obtained, corresponding to non-hydrogen bonded and hydrogen bonded OH respectively, in agreement with the previous ^{2}H solid-state NMR studies [43,45]. Thus, the majority of Ser in $(AGSGAG)_5$

or in the Cp fraction are hydrogen bonded.

It is important to note that in the repeated $(AGSGAG)_n$ structure, Ser occurs every six residues, but the lamellar structure is an eight-residue repeat. This implies that Ser does not occur at unique positions within the lamellar structure, and thus is unlikely to have a role in for example defining or stabilizing the β-turn positions. Rather, we suggest that its role is to fix one lamellar layer next to its neighbor, like a Velcro® fastener, and limit the local mobility in the layers, including of the Ala **B** location adjacent to the β-turns, which has significantly more restricted mobility in $(AGSGAG)_n$ (Figure 10). In support of this, we note that Ser residues fall into the same three groups as Ala, and are distributed through the structure in a similar way. The evidence for this statement includes:

1. There were no significant differences in the line-shapes of Ser Cβ carbons of the ^{13}C CP/MAS NMR spectra among [3-^{13}C]Ser^{9}-$(AGSGAG)_5$, [3-^{13}C]Ser^{15}-$(AGSGAG)_5$ and [3-^{13}C]Ser^{21}-$(AGSGAG)_5$ as shown in Figure S4 [34].
2. The Ser Cβ peak in the ^{13}C CP/MAS NMR spectrum of SF fiber was deconvoluted to be AP β-sheet **A**, AP β-sheet, **B** and random coil/distorted β-turn, **t** which is the same definition as that of Ala Cβ peak.19,33,34,38-40. The fraction of each conformation was determined from peak deconvolution and was approximately **t**:**A**:**B** 1:2:1, as for Ala.
3. In the 2D DARR spectrum of [U-^{13}C] Cp fraction with a 400 ms mixing time shown in Figure S5 [34], there are several correlations between Ala and Ser peaks. Namely, the Ser Cα peaks at 54.9 and 54.0 ppm (corresponding to geometries **A** and **B**, respectively) showed correlations with the Ala Cβ peaks at

19.6 and 21.7 ppm, also corresponding to geometries **A** and **B**, respectively. Especially, the Ser Cβ peak at 64.2 ppm (geometry **A**) has a strong cross peak with Ala Cβ peak, **A**, while the Ser Cβ **B** peak has correlations that are too weak to interpret. However, correlations are also seen between geometries **A** and **B**, for Ser Cβ **A** to Ala Cβ **B** and between Ser Cα and Ala Cβ. This is what is expected if Ser residues are distributed throughout the lamellar structure in the same way as Ala.

5. Conclusion

The structure and dynamics of the crystalline (Cp) fraction and the repeated Ala-Gly-Ser-Gly-Ala-Gly model peptides were studied using ^{13}C solid-state NMR and solid-state NMR relaxation methods. A lamellar structure of $(AGSGAG)_n$ in the Cp fraction with a repetitive folding using β-turns every eighth amino acid in antipolar arrangement was proposed. The Ser residues at each sixth residue form hydrogen bonds to adjacent lamellar layers and hold the layers together compactly, in a similar way to Velcro®, thereby increasing the rigidity and strength of the crystalline fraction compared to a simple $(AG)_n$ polymer.

ACKNOWLEDEMENTS

T.A. acknowledges support by a JSPS KAKENHI, Grant-in-Aid for Scientific Research (C), Grant Number JP19K05609.

Appendix A. Supplementary material

Supplementary data to this article can be found online at https://doi.

References

[1] C. Vepari, D.L. Kaplan, Silk as a biomaterial, Prog. Polym. Sci. 32 (2007) 991–1007. https://doi.org/10.1016/j.progpolymsci.2007.05.013.

[2] G.H. Altman, F. Diaz, C. Jakuba, T. Calabro, R.L. Horan, J. Chen, H. Lu, J. Richmond, D.L. Kaplan, Silk-based biomaterials, Biomaterials. 24 (2003) 401–416. https://doi.org/ 10.1016/S0142-9612(02)00353-8.

[3] L.-D. Koh, Y. Cheng, C.-P. Teng, Y.-W. Khin, X.-J. Loh, S.-Y. Tee, M. Low, E. Ye, H.-D. Yu, Y.-W. Zhang, M.-Y. Han, Structures, mechanical properties and applications of silk fibroin materials, Prog. Polym. Sci. 46 (2015) 86–110. https://doi.org/10.1016/j.progpolymsci.2015.02.001.

[4] R.F.P. Pereira, M.M. Silva, V. de Zea Bermudez, *Bombyx mori* Silk Fibers: An Outstanding Family of Materials, Macromol. Mater. Eng. 300 (2015) 1171–1198. https://doi.org/10.1002/mame.201400276.

[5] D. Kaplan, W.W. Adams, B. Farmer, C. Viney, Silk Polymers:Materials Science And Biotechnology, American Chemical Society, Washington, DC, 1994. https://doi.org/10.1021/bk-1994-0544.

[6] D. Porter, F. Vollrath, Silk as a Biomimetic Ideal for Structural Polymers, Adv. Mater. 21 (2009) 487–492. https://doi.org/10.1002/adma.200801332.

[7] F. Vollrath, D. Porter, Silks as ancient models for modern polymers, Polymer (Guildf). 50 (2009) 5623–5632. https://doi.org/10.1016/j.polymer.2009.09.068.

[8] I. Greving, M. Cai, F. Vollrath, H.C. Schniepp, Shear-Induced Self-Assembly of Native Silk Proteins into Fibrils Studied by Atomic Force Microscopy, Biomacromolecules. 13 (2012) 676–682. https://doi.org/10.1021/bm201509b.

[9] C. Guo, J. Zhang, X. Wang, A.T. Nguyen, X.Y. Liu, D.L. Kaplan, Comparative Study of Strain-Dependent Structural Changes of Silkworm Silks: Insight into the Structural Origin of Strain-Stiffening, Small. 13 (2017) 1702266.

https://doi.org/10.1002/smll.201702266.

[10] K. Yukuhiro, H. Sezutsu, N. Yonemura, Evolutionary Divergence of Lepidopteran and Trichopteran Fibroins, in: T. Asakura, T. Miller (Eds.), Biotechnol. Silk, Springer Netherlands, Dordrecht, 2014: pp. 25–47. https://doi.org/10.1007/978-94-007-7119-2_2.

[11] K. Tanaka, N. Kajiyama, K. Ishikura, S. Waga, A. Kikuchi, K. Ohtomo, T. Takagi, S. Mizuno, Determination of the site of disulfide linkage between heavy and light chains of silk fibroin produced by *Bombyx mori*, Biochim. Biophys. Acta - Protein Struct. Mol. Enzymol. 1432 (1999) 92–103. https://doi.org/10.1016/S0167-4838(99)00088-6.

[12] S. Inoue, K. Tanaka, F. Arisaka, S. Kimura, K. Ohtomo, S. Mizuno, Silk Fibroin of *Bombyx mori* Is Secreted, Assembling a High Molecular Mass Elementary Unit Consisting of H-chain, L-chain, and P25, with a 6:6:1 Molar Ratio, J. Biol. Chem. 275 (2000) 40517–40528. https://doi.org/10.1074/jbc.M006897200.

[13] C.-Z. Zhou, F. Confalonieri, N. Medina, Y. Zivanovic, C. Esnault, T. Yang, M. Jacquet, J. Janin, M. Duguet, R. Perasso, Z.-G. Li, Fine organization of *Bombyx mori* fibroin heavy chain gene, Nucleic Acids Res. 28 (2000) 2413–2419. https://doi.org/10.1093/nar/28.12.2413.

[14] C.-Z. Zhou, F. Confalonieri, M. Jacquet, R. Perasso, Z.-G. Li, J. Janin, Silk fibroin: Structural implications of a remarkable amino acid sequence, Proteins. 44 (2001) 119–122. https://doi.org/10.1002/prot.1078.

[15] B. Lotz, F.C. Cesari, The chemical structure and the crystalline structures of *Bombyx mori* silk fibroin, Biochimie. 61 (1979) 205–214. https://doi.org/10.1016/S0300-9084(79)80067-X.

[16] T. Asakura, J. Ashida, T. Yamane, T. Kameda, Y. Nakazawa, K. Ohgo, K. Komatsu, A repeated β-turn structure in Poly(Ala-Gly) as a model for silk I of *Bombyx mori* silk fibroin studied with two-dimensional spin-diffusion NMR under off magic angle spinning and rotational echo double resonance, J. Mol. Biol. 306 (2001) 291–305. https://doi.org/10.1006/jmbi.2000.4394.

[17] T. Asakura, K. Ohgo, K. Komatsu, M. Kanenari, K. Okuyama, Refinement of Repeated β-turn Structure for Silk I Conformation of *Bombyx mori* Silk Fibroin Using ^{13}C Solid-State NMR and X-ray Diffraction Methods, Macromolecules. 38

(2005) 7397–7403. https://doi.org/10.1021/MA050936Y.

[18] T. Asakura, Y. Suzuki, K. Yazawa, A. Aoki, Y. Nishiyama, K. Nishimura, F. Suzuki, H. Kaji, Determination of Accurate ^{1}H Positions of (Ala-Gly)n as a Sequential Peptide Model of *Bombyx mori* Silk Fibroin before Spinning (Silk I), Macromolecules. 46 (2013) 8046–8050. https://doi.org/10.1021/ma401531m.

[19] T. Asakura, K. Okushita, M.P. Williamson, Analysis of the structure of *Bombyx mori* silk fibroin by NMR, Macromolecules. 48 (2015) 2345–2357. https://doi.org/10.1021/acs.macromol.5b00160.

[20] R.E. Marsh, R.B. Corey, L. Pauling, An investigation of the structure of silk fibroin, Biochim. Biophys. Acta. 16 (1955) 1–34. https://doi.org/10.1016/0006-3002(55)90178-5.

[21] B. Fraser, T.P. MacRae, Conformations of Fibrous Proteins and Related Synthetic Polypeptides, Academic Press: New York, 1973.

[22] S.A. Fossey, G. Némethy, K.D. Gibson, H.A. Scheraga, Conformational energy studies of β-sheets of model silk fibroin peptides. I. Sheets of poly(Ala-Gly) chains, Biopolymers. 31 (1991) 1529–1541. https://doi.org/10.1002/bip.360311309.

[23] Y. Takahashi, M. Gehoh, K. Yuzuriha, Structure refinement and diffuse streak scattering of silk (*Bombyx mori*), Int. J. Biol. Macromol. 24 (1999) 127–138. https://doi.org/10.1016/S0141-8130(98)00080-4.

[24] T. Asakura, M. Iwadate, M. Demura, M.P. Williamson, Structural analysis of silk with ^{13}C NMR chemical shift contour plots, Int. J. Biol. Macromol. 24 (1999) 167–171. https://doi.org/10.1016/S0141-8130(98)00082-8.

[25] T. Asakura, J. Yao, T. Yamane, K. Umemura, A.S. Ulrich, Heterogeneous Structure of Silk Fibers from *Bombyx mori* Resolved by ^{13}C Solid-State NMR Spectroscopy, J. Am. Chem. Soc. 124 (2002) 8794–8795. https://doi.org/10.1021/ja020244e

[26] T. Asakura, J. Yao, ^{13}C CP/MAS NMR study on structural heterogeneity in *Bombyx mori* silk fiber and their generation by stretching., Protein Sci. 11 (2002) 2706–2713. https://doi.org/10.1110/ps.0221702.

[27] T. Asakura, R. Sugino, J. Yao, H. Takashima, K. Raghuvansh, Comparative

structure analysis of tyrosine and valine residues in unprocessed silk fibroin (silk I) and in the processed silk fiber (silk II) from *Bombyx mori* using solid-state ^{13}C, ^{15}N, and ^{2}H NMR, Biochemistry. 41 (2002) 4415–4424. https://doi.org/10.1021/bi0119013.

[28] T. Asakura, K. Suita, T. Kameda, S. Afonin, A.S. Ulrich, Structural role of tyrosine in *Bombyx mori* silk fibroin, studied by solid-state NMR and molecular mechanics on a model peptide prepared as silk I and II, Magn. Reson. Chem. 42 (2004) 258–266. https://doi.org/10.1002/mrc.1337.

[29] J. Yao, K. Ohgo, R. Sugino, R. Kishore, T. Asakura, Structural Analysis of *Bombyx mori* Silk Fibroin Peptides with Formic Acid Treatment Using High-Resolution Solid-State ^{13}C NMR Spectroscopy, Biomacromolecules. 5 (2004) 1763–1769. https://doi.org/10.1021/bm049831d.

[30] T. Asakura, K. Ohgo, T. Ishida, P. Taddei, P. Monti, R. Kishore, Possible Implications of Serine and Tyrosine Residues and Intermolecular Interactions on the Appearance of Silk I Structure of *Bombyx mori* Silk Fibroin-Derived Synthetic Peptides: High-Resolution ^{13}C Cross-Polarization/Magic-Angle Spinni, Biomacromolecules. 6 (2005) 468–474. https://doi.org/10.1021/bm049487k.

[31] T. Asakura, Y. Nakazawa, E. Ohnishi, F. Moro, Evidence from ^{13}C solid-state NMR spectroscopy for a lamella structure in an alanine-glycine copolypeptide: A model for the crystalline domain of *Bombyx mori* silk fiber, Protein Sci. 14 (2005) 2654–2657. https://doi.org/10.1110/ps.051525505.

[32] T. Asakura, H. Sato, F. Moro, Y. Nakazawa, A. Aoki, Lamellar Structure in Poly(Ala-Gly) Determined by Solid-State NMR and Statistical Mechanical Calculations, J. Am. Chem. Soc. 129 (2007) 5703–5709. https://doi.org/10.1021/ja070128h.

[33] Y. Suzuki, A. Aoki, Y. Nakazawa, D.P. Knight, T. Asakura, Structural Analysis of the Synthetic Peptide (Ala-Gly-Ser-Gly-Ala-Gly)$_5$, a Model for the Crystalline Domain of *Bombyx mori* Silk Fibroin, Studied with ^{13}C CP/MAS NMR, REDOR, and Statistical Mechanical Calculations, Macromolecules. 43 (2010) 9434–9440. https://doi.org/10.1021/ma1018878.

[34] K. Okushita, A. Asano, M.P. Williamson, T. Asakura, Local Structure and Dynamics of Serine in the Heterogeneous Structure of the Crystalline Domain of *Bombyx mori* Silk Fibroin in Silk II Form Studied by 2D ^{13}C–^{13}C Homonuclear

Correlation NMR and Relaxation Time Observation, Macromolecules. 47 (2014) 4308–4316. https://doi.org/10.1021/ma500908m.

[35] T. Asakura, Y. Sato, A. Aoki, Stretching-Induced Conformational Transition of the Crystalline and Noncrystalline Domains of ^{13} C-Labeled *Bombyx mori* Silk Fibroin Monitored by Solid State NMR, Macromolecules. 48 (2015) 5761–5769. https://doi.org/10.1021/acs.macromol.5b01365.

[36] T. Asakura, T. Ohata, S. Kametani, K. Okushita, K. Yazawa, Y. Nishiyama, K. Nishimura, A. Aoki, F. Suzuki, H. Kaji, A.S. Ulrich, M.P. Williamson, Intermolecular Packing in *B. mori* Silk Fibroin: Multinuclear NMR Study of the Model Peptide (Ala-Gly) $_{15}$ Defines a Heterogeneous Antiparallel Antipolar Mode of Assembly in the Silk II Form, Macromolecules. 48 (2015) 28–36. https://doi.org/10.1021/ma502191g.

[37] T. Asakura, A. Aoki, K. Komatsu, C. Ito, I. Suzuki, A. Naito, H. Kaji, A Lamellar Structure in Alanine-Glycine Copolypeptides Studied by Solid-State NMR Spectroscopy: A Model for the Crystalline Domain of *Bombyx mori* Silk Fibroin in Silk II Form, Biomacromolecules. 21 (2020) 3102-3111. https://doi.org/10.1021/acs.biomac.0c00486.

[38] D.J. Strydom, T. Haylett, R.H. Stead, The amino-terminal sequence of silk fibroin peptide Cp - A reinvestigation., Biochem. Biophys. Res. Commun. 79 (1977) 932–938. https://doi.org/10.1016/0006-291X(77)91200-1.

[39] A. Naito, Y. Tasei, A. Nishimura, T. Asakura, Packing Arrangements and Intersheet Interaction of Alanine Oligopeptides As Revealed by Relaxation Parameters Obtained from High-Resolution ^{13}C Solid-State NMR, J. Phys. Chem. B. 121 (2017) 8946–8955. https://doi.org/10.1021/acs.jpcb.7b07068.

[40] A. Naito, Y. Tasei, A. Nishimura, T. Asakura, Unusual Dynamics of Alanine Residues in Polyalanine Regions with Staggered Packing Structure of Samia cynthia ricini Silk Fiber in Dry and Hydrated States Studied by ^{13}C Solid-State NMR and Molecular Dynamics Simulation, J. Phys. Chem. B. 122 (2018) 6511–6520. https://doi.org/10.1021/acs.jpcb.8b03509.

[41] T. Asakura, Y. Tasei, H. Matsuda, A. Naito, Dynamics of Alanine Methyl Groups in Alanine Oligopeptides and Spider Dragline Silks with Different Packing Structures As Studied by ^{13}C Solid-State NMR Relaxation, Macromolecules. 51 (2018) 6746–6756.

https://doi.org/10.1021/acs.macromol.8b01402.

[42] D.A. Torchia, The measurement of proton-enhanced carbon-$^{13}T_1$ values by a method which suppresses artifacts, J. Magn. Reson. 30 (1978) 613–616. https://doi.org/10.1016/0022-2364(78)90288-3.

[43] T. Kameda, Y. Ohkawa, K. Yoshizawa, J. Naito, A.S. Ulrich, T. Asakura, Hydrogen-Bonding Structure of Serine Side Chains in *Bombyx mori* and *Samia cynthia ricini* Silk Fibroin Determined by Solid-State ^{2}H NMR, Macromolecules. 32 (1999) 7166–7171. https://doi.org/10.1021/ma990554q.

[44] T. Yamane, K. Umemura, T. Asakura, The structural characteristics of *Bombyx mori* silk fibroin before spinning as studied with molecular dynamics simulation, Macromolecules. 35 (2002) 8831–8838. https://doi.org/10.1021/ma0209390.

[45] H. Saito, R. Tabeta, A. Kuzuhara, T. Asakura, A ^{2}H NMR Study of [*Ser*-3,3-$^2H_2$]- and [*Ala*-3,3,3-$^2H_3$]- Silk Fibroins in the Solid State. Role of Side-Chain Moiety in Stabilization of Secondary Structure, Bull. Chem. Soc. Jpn. 59 (1986) 3383–3387 https://doi.org/10.1246/bcsj.59.3383.

[46] H. Saito, M. Yokoi, M. Ishida, T. Asakura, M. Yokoi, T. Asakura, Dynamic Features of Side Chains in Tyrosine and Serine Residues of Some Polypeptides and Fibroins in the Solid as Studied by High-Resolution Solid-State ^{13}C NMR Spectroscopy, Macromolecules. 23 (1990) 83–88. https://doi.org/10.1021/ma00203a016.

[47]. Naito, A.; Ganapathy, S.; Akasaka, K.; McDowell, C. A. Spin-Lattice Relaxation of ^{13}C in Solid Amino Acids Using CP-MAS Technique. J. Magn. Reson. 54 (1983) 226-235. https://doi.org/10.1016/0022-2364(83)90045-8.

[48]. Lehmann, M. S.; Koetzle, T. F.; Hamilton, W. C. Precision Neutron Diffraction Structure Determination of Protein and Nucleic Acid Components. I. Crystal and Molecular Structure of the Amino Acid L-Alanine. J. Am. Chem. Soc. 94 (1972) 2657-2660. https://doi.org/10.1021/ja00763a016.